Available online at www.sciencedirect.com
SCIENCE DIRECT®
Journal of Catalysis 225 (2004) 240–248
JOURNAL OF CATALYSIS
www.elsevier.com/locate/jcat

Nature of the vanadia–ceria interface in V^{5+}/CeO_2 catalysts and its relevance for the solid-state reaction toward $CeVO_4$ and catalytic properties

M.V. Martínez-Huerta,[a] J.M. Coronado,[a] M. Fernández-García,[a] A. Iglesias-Juez,[a] G. Deo,[b] J.L.G. Fierro,[a] and M.A. Bañares[a,*]

[a] *Instituto de Catálisis y Petroleoquímica, CSIC; Campus Cantoblanco, E-28049 Madrid, Spain*
[b] *Department of Chemical Engineering, Indian Institute of Technology Kanpur, Kanpur 208 016, India*

Received 11 February 2004; revised 5 April 2004; accepted 8 April 2004

Abstract

A combination of in situ Raman, XANES, and EPR spectroscopies is used to study the nature of the interaction between V and Ce in the ceria-supported vanadia catalysts. Vanadium oxide species disperse on ceria up to 9 V atoms/nm^2 of support. Surface V^{5+} species closely interacts with ceria support promoting a reduction of surface Ce^{4+} to Ce^{3+}. Upon heating or during reaction surface vanadia reacts with ceria support forming a $CeVO_4$ phase. The active site appears to be V^{5+}–O–Ce^{3+} for both systems. The redox cycle for oxidative dehydrogenation appears to be associated with Ce, rather than with V sites.

Keywords: In situ; Raman; XANES; EPR; Vanadia; Ceria; Solid-state reaction; $CeVO_4$; Vanadate

1. Introduction

Total oxidation reactions account for the majority of uses of CeO_2-containing materials in catalysis [1]. The redox properties of ceria and the high lability of its lattice oxygen are among the most important factors that contribute to the catalytic reactivity of CeO_2 in oxidation reactions; in particular, for total oxidation reactions. However, the catalytic behavior of CeO_2 can be modified by the addition of dopants that interact with the ceria support [1]. The presence of vanadia on ceria affords interesting performances for oxidative dehydrogenation (ODH) reactions [2,3]. In general, supported vanadia catalysts are one of the most active and attractive catalysts for light alkane ODH [4–8]. Several studies address the structure and the oxidation state of supported vanadia catalysts during hydrocarbon oxidation reactions [9–11]. The in situ Raman and UV–vis–NIR studies under reaction conditions provide new insights into the behavior of surface vanadia species during hydrocarbon oxidation reactions: (i) the dehydrated surface V^{5+} species appears to be the predominant surface species, and (ii) the extent of reduction of the surface vanadia species depends on the reducing power of the hydrocarbon, the specific oxide support, and the ratio of polymeric to isolated surface vanadia species [11,12]. The surface polymeric vanadia species on ceria are more reducible than the isolated ones, according to in situ Raman spectroscopy [13]. There is not much information available about the nature of surface vanadium oxide species on ceria [2,3,12–14]. In general, the interfaces between a metal oxide supported on a metal oxide substrate have been less studied that the interfaces between metal and metal oxide substrates [15]. During alkane oxidation reactions, the conversion decreases due to deactivation, which appears related to the formation of $CeVO_4$ [3,12]. However, detailed information about the nature of the vanadia–ceria interface is scarce. In situ Raman, XANES, and EPR spectroscopies are used to afford some understanding about this interaction.

* Corresponding author. Instituto de Catálisis y Petroleoquímica, CSIC Marie Curie, 2, E-28049, Madrid, Spain. Fax: +34 91 585 4760.
E-mail address: mbanares@icp.csic.es (M.A. Bañares).

0021-9517/$ – see front matter
doi:10.1016/j.jcat.2004.04.005

2. Experimental

2.1. Catalyst synthesis

The vanadium oxide was supported on CeO_2 (Engelhard; 36 m^2/g) according to the experimental procedure described elsewhere [2]. Essentially, the catalysts were prepared by incipient wetness impregnation with V-isopropanol in a glove box with nitrogen flow. The impregnated samples were kept at room temperature overnight in the glove box. Then the samples were dried at 120 °C for 1 h and at 300 °C another 1 h with nitrogen flow. Finally, the samples were calcined at 300 °C for 1 h and 450 °C for 2 h in flowing oxygen. The catalysts are referred to as "*x*VCe," where "*x*" represents the weight percent of V_2O_5 on CeO_2. The monolayer coverage of vanadia on alumina is understood as the dispersion limit loading, i.e., the maximum vanadia loading on alumina that can be supported as surface vanadia species; V_2O_5 aggregates form above this loading crystalline. Raman spectroscopy is use to determine this monolayer coverage, since it can readily detect V_2O_5 crystallites. The maximum loading of vanadia free of crystalline V_2O_5 was 4% V_2O_5/CeO_2, which corresponds to 9 V atom/nm^2 of ceria support.

2.2. Oxidative dehydrogenation of ethane

Ethane oxidation was carried out in an isothermal fixed-bed reactor. The catalysts (20 mg) were evaluated in the 450 to 610 °C temperature range, at atmospheric pressure. The reaction gas mixture consisted of $C_2H_6/O_2/He$ (1/2/8) and was used with a total flow rate of 30 cm^3/min. The reactor consisted of a quartz tube of 6 mm o.d. (4 mm i.d.) where no void volume was permitted by using a 4 mm o.d. quartz tube insert to avoid homogeneous reaction from the gas phase.

2.3. Laser Raman spectroscopy

The in situ Raman spectra were obtained with a Renishaw Micro-Raman System 1000 equipped with a cooled CCD detector (−73 °C) and a holographic super-Notch filter that removes the elastic scattering. The samples were excited with the 514 nm Ar line in an in situ cell (Linkam, TS-1500), which allows temperature treatments up to 1500 °C under flowing gases. The samples were in powder form to prevent diffusion problems and ensure that all catalyst in the cell is exposed to the flowing gases. The spectral resolution is 3 cm^{-1}, and the spectra acquisition consisted of five accumulations of 60 s. The samples for the in situ measurements were pretreated in O_2/He at 450 °C for 1 h before any further treatment. In situ spectra during temperature treatments are taken at high temperature, during a stepwise heating. Raman spectroscopy provides molecular information about the bulk of the material for it penetrates ca. 1 μm.

2.4. XANES data

XANES data at the V *K edge* were measured on line 9.3 of the SRS synchrotron at Daresbury, UK. A Si(111) double-crystal monochromator was used with a detuning of ca. 60% to minimize the harmonic content of the beam. Transmission experiments were carried out using N_2/O_2-filled ionization chambers. The energy scale was simultaneously calibrated by measuring the corresponding metal foil inserted before a third ionization chamber. Samples as self-supporting disks (absorbance 1.5) were place in a controlled-atmosphere cell developed at the 9.3 beamline for treatment. XANES spectra were taken at the temperature and under the controlled atmosphere (e.g., $C_2H_6/O_2/He = 1/2/8$ or dry air) indicated for each case.

2.5. EPR measurements

EPR measurements were carried out at 77 K with a Brüker ER200D spectrometer provided with a T-type double cavity and operating in the X band (9.55 GHz). Frequency calibration was performed using a DPPH standard ($g = 2.0036$). All the spectra were recorded at −196 °C using a microwave power of 19 mW. Computer simulations were used when necessary to check spectral parameters. Aliquots of the catalyst (30–40 mg) were placed into a quartz probe cell with greaseless stopcocks, which can be externally heated with a tubular furnace. All the samples were pretreated in oxygen at 300 °C for 1 h and subsequently outgassed at the same temperature for 1 h. Oxygen adsorption experiments were carried out in a conventional high vacuum line made of Pyrex, which is able to achieve dynamic pressures lower than 2×10^{-2} N m^2. A fixed dose (≈ 100 μmol per gram of sample) of this gas (L'Air Liquide; 99.9%) was admitted in the cell at 77 K, and subsequently the sample evacuated at the same temperature for 30 min in order to remove weakly adsorbed (physisorbed) oxygen, which could lead to the broadening of the signals by dipolar interactions.

3. Results

3.1. Activity study

Table 1 shows the steady-state ethane oxidative dehydrogenation data for the VO*x*/CeO_2 catalysts at different reaction temperatures. $CeVO_4$ is also included as a reference. The catalysts show some deactivation during time on stream, which is more intense at higher vanadia loading, during the first couple of hours. In the absence of vanadium, pure ceria is extremely reactive; however, the main product is CO_2. Ethane conversion values are below 70% in the 510–590 °C reaction temperature range due to oxygen-limiting conditions. The performance is dramatically different upon addition of vanadium. With 1% V_2O_5/CeO_2 (i.e., 1/5 monolayers) the activity decreases to very low conversion values,

Table 1
Ethane ODH on xVCe catalysts including CeO_2 and $CeVO_4$ references

Catalyst	T (°C)	Conversion (%)	Selectivity (%)		
			C_2H_4	CO_2	CO
CeO_2	510	61.1	4	96	0
1VCe		1.4	35	65	0
2VCe		1.3	64	36	0
3VCe		0.7	69	25	6
4VCe		1.0	52	6	42
5VCe		1.0	44	8	48
$CeVO_4$		1.7	42	32	26
CeO_2	550	66.2	4	96	0
1VCe		5.0	28	64	8
2VCe		3.2	44	16	45
3VCe		3.6	46	13	41
4VCe		2.6	50	6	44
5VCe		2.9	43	12	45
$CeVO_4$		4.1	27	20	52
CeO_2	590	68.4	5	95	0
1VCe		19.6	20	54	27
2VCe		8.6	38	11	50
3VCe		8.7	35	13	53
4VCe		7.3	44	7	49
5VCe		5.9	42	14	45
$CeVO_4$		7.4	27	22	51

Reaction conditions: 20 mg, 30 ml/min, $C_2H_6/O_2/He = 1/2/8$ molar ratio.

and the product distribution shifts from combustion to ODH. The formation of CO_2 decreases with vanadia loading on ceria. For a given reaction temperature, conversion decreases and the ethylene selectivity increases with vanadia loading on ceria. 1VCe exhibits a product distribution that resembles a linear combination of those of ceria and $CeVO_4$, but the product distribution is closer to that of $CeVO_4$ if vanadia loading is higher.

3.2. Raman study

The in situ Raman spectrum at 300 °C of dehydrated fresh 3VCe catalyst is shown in Fig. 1. The Raman spectrum of reference $CeVO_4$ (Alfa, 99.9%) is shown in Fig. 1d. Pure CeO_2 (Fig. 1a) exhibits an intense Raman band at 460 cm^{-1}, and smaller bands at 239 and 590 cm^{-1}. The dehydrated fresh catalyst (Fig. 1b) exhibits a Raman band at 1027 cm^{-1}, characteristic of the terminal V=O bond of the dehydrated surface vanadia species [11]. The Raman band near 940 cm^{-1} is assigned to the active stretching mode of V–O–V functionality of surface polymeric vanadia [11]. The Raman bands characteristic of the terminal V=O and V–O–V bonds of the surface vanadia species, are sensitive to hydration; this hydration–dehydration process of the supported vanadia catalysts is completely reversible at 300 °C [16]. The dehydrated used 3VCe catalyst (Fig. 1c) exhibits the Raman band at 1026 cm^{-1} characteristic of the terminal V=O bond, and new Raman features that become more intense with vanadia loading. The new Raman bands at 260, 779, 799, and 854 cm^{-1} are the most intense Raman bands of $CeVO_4$: 214, 260, 368, 460, 785, 798, and 841 cm^{-1}. The Raman band at 841 cm^{-1} is assigned to A1g vanadate symmetric stretching (ν_1), at 798 and 785 to the Eg and B2g antisymmetric stretching of vanadates (ν_3), at 460 and 368 cm^{-1} to B2g and B1g deformations (ν_4 and ν_2, respectively) [17]. The formation of $CeVO_4$ on ceria-supported vanadia catalysts used for propane ODH reaction has also been reported [3].

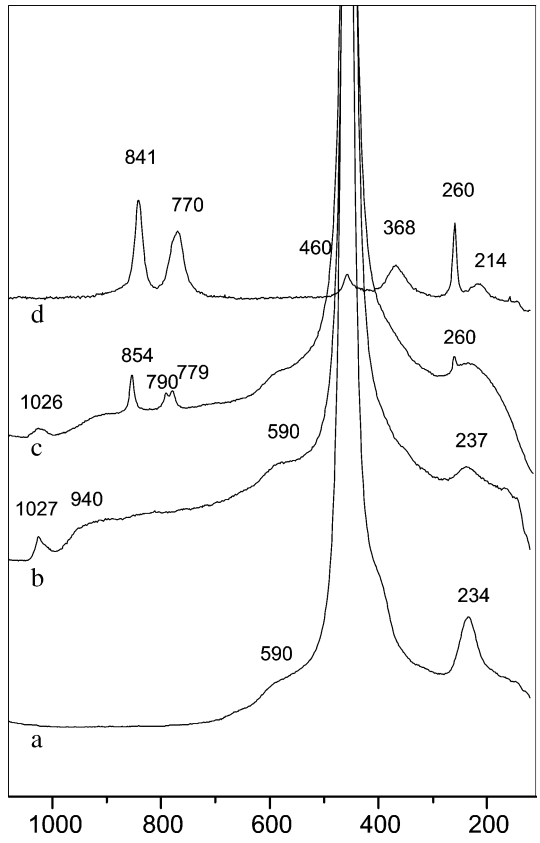

Fig. 1. In situ Raman spectra of (a) reference CeO_2, (b) dehydrated fresh 3VCe, (c) dehydrated used 3VCe, and (d) reference $CeVO_4$.

3.3. In situ oxidizing environments

Dehydrated catalysts were heated stepwise in the in situ Linkam cell in a dry air stream. Every catalyst exhibited a solid-state reaction forming $CeVO_4$. Fig. 2 illustrates the temperature-programmed Raman (TP-Raman) study of 1VCe in dry air. The surface dehydrated structures of vanadia do not change up to 450 °C. Two Raman bands at 1017 and 1034 cm^{-1} correspond to the V=O modes of surface isolated and polymeric vanadia species, respectively [11,13]. At 500 °C and above, the Raman bands of the surface vanadia species become weaker. Such weakening is not due to thermal broadening since other supported vanadia oxide species show very moderate effects on the V=O vibration at high temperature [11]. Near 700 °C, the Raman band of the V=O mode is hardly visible and new Raman features become apparent near 765 and 839 cm^{-1}. These new Ra-

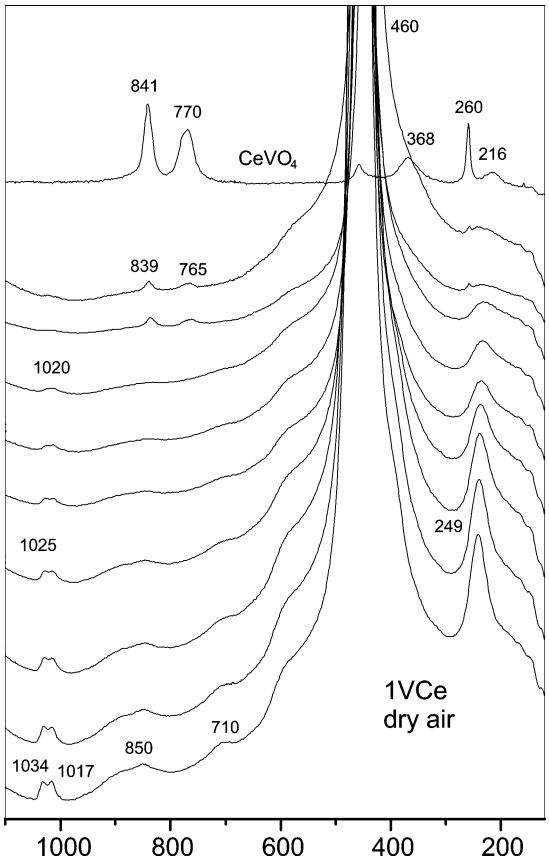

Fig. 2. Raman study during temperature-programmed heating of fresh dehydrated 1VCe in dry air. Spectra taken at the temperature indicated in the figure.

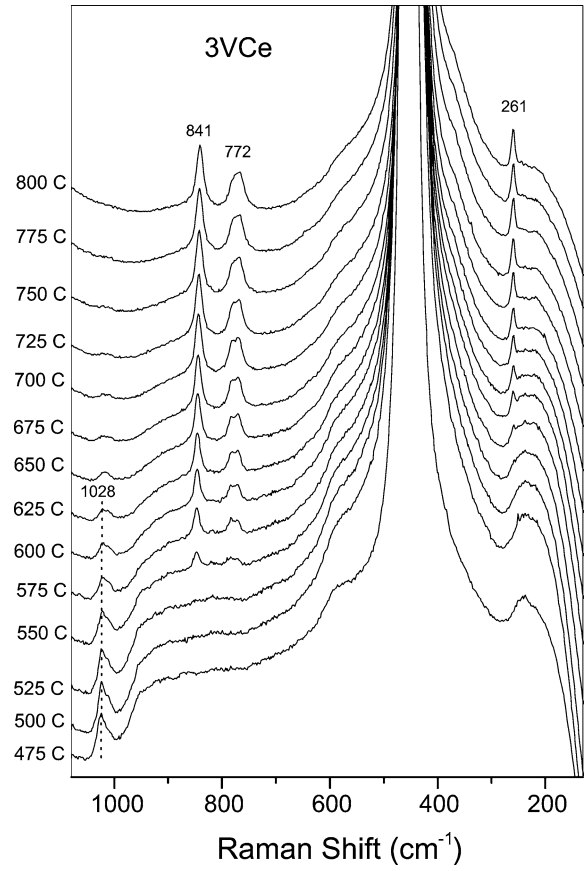

Fig. 3. Raman study during temperature-programmed heating of fresh dehydrated 3VCe in dry air. Spectra taken at the temperature indicated in the figure.

man bands are the most intense ones for $CeVO_4$. Fig. 3 illustrates the TP-Raman study of 3VCe in dry air. Surface vanadia species on ceria show a Raman band at 1028 cm^{-1}, characteristic of the V=O mode of surface vanadia species. The two V=O modes of surface isolated and polymeric vanadia species appear to coalesce in a single Raman band if vanadia coverage is above ca. 20% monolayer coverage [11]. No important changes in the Raman spectra are evident up to 525 °C in air. However, new Raman features at 772 and 841 cm^{-1} (due to $CeVO_4$) become apparent near 550 °C. There is an important decrease of the Raman bands of surface vanadia species at 650 °C, and no surface vanadia species appear to be present at 800 °C. A detailed close-up of the surface vanadia spectral window is presented in Fig. 4 for 4VCe during TP-Raman study. In this case, the formation of $CeVO_4$ starts at 400 °C and the removal of surface vanadia species is complete by 550 °C. The solid-state reaction between surface vanadia and ceria starts at 450 °C in 5VCe and no surface vanadia species remain visible by 575 °C (Fig. 5). In summary, the Raman bands of $CeVO_4$ phase are detected by Raman above 700 °C for 1VCe, around 550 °C for 3VCe, and near 450 °C for both 4VCe and 5VCe in dry air. Therefore, the $CeVO_4$ detection temperature by in situ Raman in an oxidizing environment decreases with increasing vanadium loading in the ceria-supported vanadia catalysts.

3.4. XANES study

The in situ vanadium *K-edge* XANES profile for the 5VCe sample under in situ conditions is presented in Fig. 6. The dehydrated catalyst in air at 300 °C presents an essentially featureless spectrum (Fig. 6a), indicative of a strong disorder at the local level [18]. However, a comparison with the V^{5+} reference systems (see the derivative spectra in the inset of Fig. 6) points out to a reasonable resemblance to that of $CeVO_4$, particularly in the preedge region. This suggests that the V–O distance and local coordination symmetry are rather similar in both systems [18,19]. The low signal-to-noise ratio at 300 °C does not allow, on the other hand, a reliable EXAFS study of the V-local order. As XANES is only sensitive to local order, this would indicate that V in the dehydrated state at 300 °C has a significant number of different local structures at the ceria surface but that most of them have Ce ions in close neighborhood such that there is an influence on the V–O distance and on the local environment in a way that resembles the $CeVO_4$ phase. The characteristic $CeVO_4$ XANES shape only develops at higher temperatures, providing evidence that the V^{5+}-containing phase forms under reaction conditions, gaining at the same time homogeneity at a local level for the V local environment. The XANES spectra displayed in Figs. 6b and c give evidence of the sta-

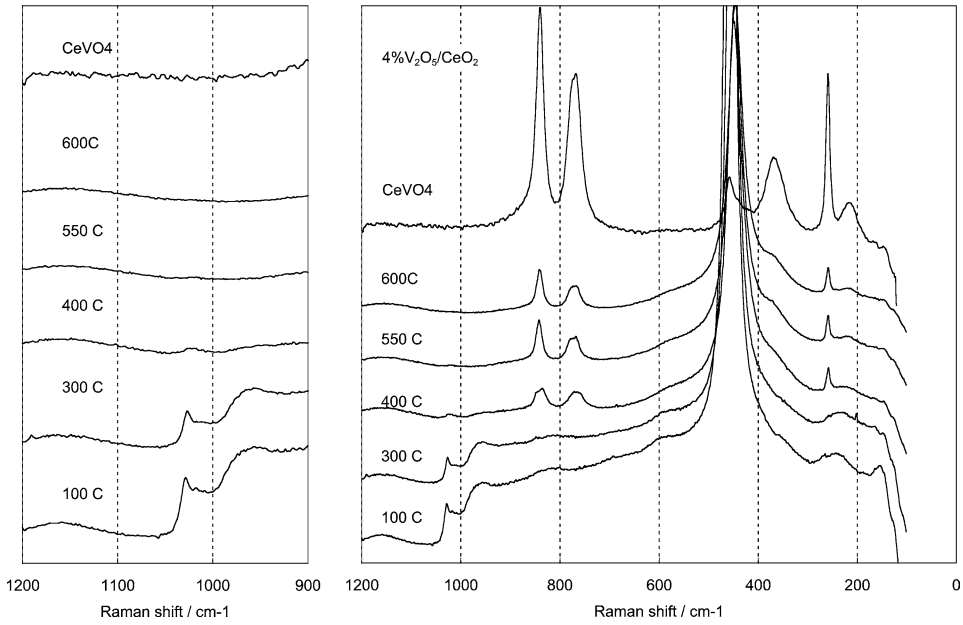

Fig. 4. Raman study during temperature-programmed heating of fresh dehydrated 4VCe in dry air. Spectra taken at the temperature indicated in the figure. The left panel shows a blowup of the 900–1200 cm^{-1} window, characteristic of the V=O and V–O–V vibration modes of surface vanadia species.

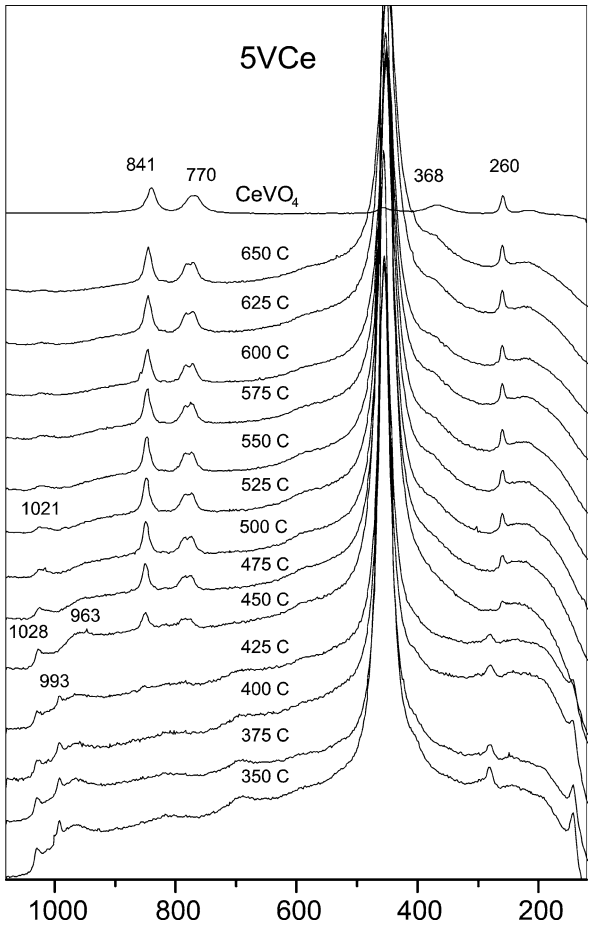

Fig. 5. Raman study during temperature-programmed heating of fresh dehydrated 5VCe in dry air. Spectra taken at the temperature indicated in the figure.

bility of the V–Ce binary phase in either ODH conditions or under air at high temperature.

3.5. EPR study of oxygen adsorption

The EPR spectra of the VCe samples calcined and outgassed at 300 °C present a series of very weak lines near $g_{\parallel} = 1.94$ and $A_{\parallel} = 13 \times 10^{-3}$ cm^{-1}, which can be attributed to the hyperfine structure of residual isolated VO^{2+} groups (^{51}V nuclear spin $I = 7/2$; natural abundance 99.75%) [20–23]. Similar signals have previously been detected in V_2O_5/CeO_2 materials treated at temperatures lower than those required for the formation of $CeVO_4$ [21–23]. In addition, the samples that contain CeO_2 typically show a sharp axial signal with $g_{\perp} = 1.965$ and $g_{\parallel} = 1.940$. These features have been previously related with either quasi-free electrons or with Ce^{3+} cations located in distorted sites of the fluorite lattice [21–24]. A recent study has assigned this signal to Cr^{3+} impurities of CeO_2 at the ppb level [25]. In any case, these centers of the CeO_2 do not seem to be relevant for the surface reactivity of the VCe catalysts, and therefore they will not be further discussed. On the other hand, the EPR spectra of the $CeVO_4$ sample treated in vacuum at 300 °C do not show any signal. EPR monitoring of the oxygen adsorption has been frequently used as a method to study the surface redox characteristics of samples containing cerium [26,27]. Reduced cerium centers (Ce^{3+}) are not easily detectable due to their short relaxation time [26]; however, it will be possible to reveal indirectly their presence at the surface by titration with oxygen. This procedure is based on the fact that the following reaction readily occurs upon oxygen adsorption if the Ce^{3+} centers are coordinatively

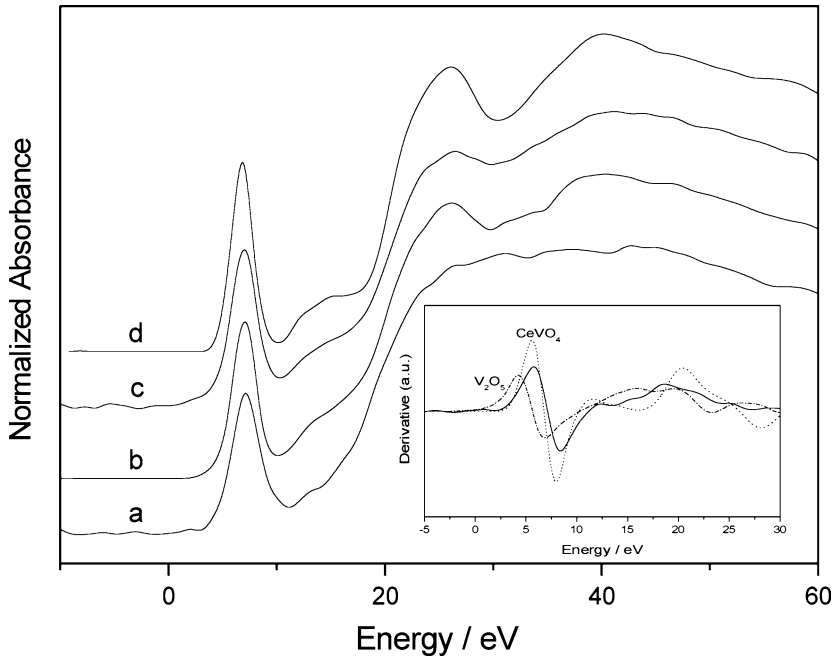

Fig. 6. XANES profiles of the *K edge* of vanadium of (a) 5VCe at 300 °C, (b) 5VCe during ethane ODH reaction condition at 800 °C, (c) 5VCe at 800 °C under air after ethane ODH, and (d) reference $CeVO_4$. Inset: derivative spectra of a and reference compounds.

unsaturated:

$$Ce^{3+} + O_2 \rightarrow Ce^{4+}\text{–}O_2{}^{-}. \quad (1)$$

The resulting surface complexes, Ce^{4+}–$O_2{}^{-}$, can be detected by EPR spectroscopy, and the characteristic of the signals can provide valuable information about the chemical nature of the reduced cerium centers [26–29]. It has been previously found that the presence of metal ions other than cerium (e.g., Al, Zr, Ti) in the second coordination sphere results in a shift of the g_x component, following the axes ascription reported elsewhere to a lower magnetic field [26–30]. This behavior has been related to an increasing covalent character of the bond between the π^* orbitals of the superoxide fragment and the lanthanide cation [26,27,29,30]. This would lower the efficiency of the charge transference between the surface and the adsorbed oxygen. On the other hand, the signal with g_x closer to g_e (2.0023) has been attributed to superoxide species attached to Ce centers with reduced coordination, which are preferentially formed in the (111) plane of the CeO_2 [26].

The EPR spectrum of the reference CeO_2 sample pretreated at 300 °C and contacted with oxygen at −196 °C is displayed in Fig. 7a. A pseudo-axial signal, C1, with approximate components at $g_\parallel = 2.035$ and $g_\perp = 2.011$ is the main contribution to the spectrum, although a second signal, C2, with a component at ca. $g = 2.008$ can be also envisaged. In accordance with the literature, these lines can be assigned to superoxide species adsorbed on more (signal C1) and less (signal C2) coordinatively saturated Ce^{4+} sites of the surface [26,27,29,30]. On the other hand, the spectrum of pure $CeVO_4$ (see Fig. 7b) submitted to the same treatment is shown in Fig. 7b, and it consists of a single axial

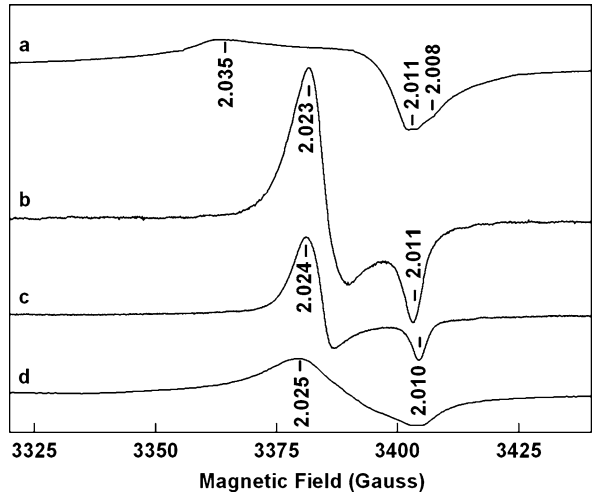

Fig. 7. EPR spectra of the samples (a) CeO_2, (b) $CeVO_4$, (c) 5VCe, and (d) 1VCe calcined in O_2 at 300 °C, outgassed at the same temperature and subsequently contacted with 100 μmol of O_2 at −196 °C.

signal, CV1, which can be simulated having $g_\perp = 2.023$ and $g_\parallel = 2.011$. On the basis of the absence of hyperfine structure, and considering that the obtained parameters are significantly larger than g_e [26–31], it can be concluded that signal CV1 are not related with V centers but with cerium cations at the $CeVO_4$ surface. In fact, Ce^{4+}–$O_2{}^{-}$ species formed at low CeO_2 coverage on γ-Al_2O_3 give rise to axial signals similar to CV1 [26,30]. This observation is not surprising considering that in this mixed oxide, vanadium presents its maximum oxidation state (V^{5+}), and therefore it can hardly donate electronic density to the oxygen molecules as to form superoxide radicals, as described by Eq. (1). Ac-

cording with the usual interpretation, the shift of g_x, which is equivalent to $g_\perp$ for signal VC1, represents an increase of the degree of covalency of the bond of the superoxide fragment with the metal [26–30]. Consequently, a delocalization of the electron between the three centers rather than the formation a purely ionic Ce^{4+}–O_2^- adduct could better describe the electronic configuration of the species generating signal VC1. Since the transferred electron is located in an antibonding orbital, this process contributes to activate the oxygen molecules. Near one-third of these superoxide radicals remain at the $CeVO_4$ surface after heating the sample to room temperature (RT); however, these species are weakly bound as they are easily removed following a short outgassing at RT.

The EPR spectra of the samples 1VCe and 5VCe pretreated at 300 °C and contacted with oxygen at 300 °C are also plotted in Fig. 7. In the case of sample 1VCe a signal, VC2, with approximate parameters $g_z = 2.025$, $g_x = 2.022$, and $g_y = 2.011$ is observed; 5VCe exhibits an axial signal, VC3, with parameters $g_\perp = 2.024$ and $g_\parallel = 2.010$. The amplitude of these lines increases with vanadium content. On the basis of the similarity of parameters of these signals with those of VC1, lines of the type VC2 and VC3 can be attributed to superoxide species adsorbed on cerium centers that share an oxide anion with a vanadium atom. The present data suggest that Ce^{3+}–O^{2-}–V^{5+} sites form when vanadia is well-dispersed on the CeO_2 support. These Ce^{3+}–O^{2-}–V^{5+} sites can be considered precursors of a well-developed $CeVO_4$. On the other hand, the intensity of the weak signals associated with VO_2^+ is not significantly affected by oxygen adsorption. For these VCe samples, it can be concluded that the activation of oxygen molecules takes place at the sites formed by cerium surface atoms modified by vanadium atoms located in the coordination sphere (i.e., Ce^{3+}–O^{2-}–V^{5+}).

4. Discussion

The activity of CeO_2 decreases upon vanadia addition, mainly due to a reduction of CO_2 formation. The combustion properties of CeO_2 are due to highly reactive oxygen species. The possibility of readily switching between Ce^{3+} and Ce^{4+} and the high lability of lattice oxygen are well known [1,32,33]; they are among the most important factors which contribute to the catalytic reactivity of CeO_2 in total oxidation reactions. They also appear to be the driving force for V–Ce oxide interface interaction [34]. The dramatic effect of V, even at very low monolayer coverage, suggests that surface vanadium oxide species must preferentially titrate the most reactive sites at the surface of CeO_2.

As vanadia coverage on ceria increases, the product distribution approaches that of $CeVO_4$. The used catalysts present Raman bands of $CeVO_4$. This trend becomes more evident as vanadium loading increases. These catalysts exhibit a change in their structure and performance during ethane ODH. Such a change appears related to the deactivation of the catalyst, which is mainly due to a decrease in CO_2 formation. Vanadia loading and calcination temperature promote the formation of and/or sintering of $CeVO_4$ aggregates in ceria-supported vanadia. The temperature for this phenomenon in air decreases with vanadia loading. It is interesting to underline that surface V^{5+} species are not restored upon reoxidation (Raman band at 1026 cm^{-1}) in this study. A reversible formation of $CeVO_4$ has been reported [3]. In that case, surface vanadia species are restored upon hydration. That $CeVO_4$ phase is very incipient (very weak Raman features) and it makes sense that the formation of $CeVO_4$ may be reversible. Such precursor of the $CeVO_4$ phase, here detected by XANES and EPR, can be viewed as surface V species at chemically interacting distances with Ce^{3+} ions and having V–O first coordination distance and local symmetry rather close to those of the well-formed binary phase. However, the $CeVO_4$ phase formed here at higher temperatures (and detected by Raman) must possess larger domains (sharper Raman bands) and show no reversibility. The latter might be ascribed to the formation of bulk-like aggregates during the sintering of V-containing species. The absence/presence of V–O–V links under such phase may explain the reversibility or not under hydration. The nature of V–Ce oxide interaction appears to affect the redox state of the ceria upon exposure to reducing environments [1,33,34]. Interestingly, considerable amount of surface Ce^{3+} species remain after exposures to oxygen in bulk ceria [33], being particularly true for nanosized materials [35]. The surface Ce^{3+} (chemical) state stability could be further enhanced by interaction with another element, like vanadium. Wong and Vohs show that surface Ce^{4+} reduces to Ce^{3+} oxidizing vanadium atoms on CeO_2(111) [34]. It thus appears that V limits the easy valence state switching of the Ce^{4+}/Ce^{3+}` redox pair, characteristic of ceria, by enhancing the energy stability of the Ce^{3+} chemical state.

The fact that the selectivity trends are rather similar between ceria-supported vanadia and $CeVO_4$ would suggest that the active site in both types of systems is the same. The only common functionality is the V–O–Ce bond. However, Ce sites are Ce^{4+} in CeO_2 support but Ce^{3+} in $CeVO_4$. The difference in oxidation state of Ce in V–O–Ce bonds would suggest a different reactivity. Since, the performance is rather similar for both systems, it would imply that vanadia affects surface ceria sites that may become trivalent upon coordination with surface vanadia species. The EPR and XANES results provide evidence that this may be the case while XANES additionally shows no appreciable reduction of V^{5+} sites. Therefore, the V–O–Ce bond in both ceria-supported vanadia and $CeVO_4$ would be V^{5+}–O–Ce^{3+}; although, as said before, a lack of medium- and long-range order is present in the ceria-supported vanadia at low temperatures. In this "precursor" state, oxygen related properties would follow those of the $CeVO_4$ phase while V may maintain to a certain degree the characteristics typical of isolated species and differ from those of the above-noted phase. Note

that, as said before, the lack of medium- and long-range order of such a precursor state makes it Raman silent.

$CeVO_4$ is present in used catalysts even when they operate at reaction temperatures lower than that required for bulk $CeVO_4$ formation. The formation of a well-developed $CeVO_4$ phase is promoted by ODH conditions; this may be due to the consecutive cycles of oxidation/reduction. The oxidation state in $CeVO_4$ are V^{5+} and Ce^{3+} and XANES show no appreciable reduction of V^{5+} during reaction, it thus makes sense to assume that the *catalytic redox cycle on ceria-supported vanadia may be due to the redox cycle of cerium near vanadium*; unlike most supported vanadia catalysts, which work on the redox cycle of vanadium sites. A similar trend is observed in ceria-supported chromia catalysts [36]. The EPR data also favor this interpretation. The interaction of CeO_2 with vanadia also stabilizes surface Ce^{3+} sites, concomitantly moderating the valence change ability of the Ce^{4+}/Ce^{3+} pair, as well as blocking the corresponding V redox interplay. Vanadia thus modulates the reactivity of surface ceria sites, which would account for the shift in the performance of ceria from combustion to ODH, while ceria blocks V redox behavior.

Although limited in its capacity, the redox cycle of Ce^{3+} sites during ethane ODH reaction would be the driving force to enable the formation of $CeVO_4$ at temperatures lower than those observed in air. This may be the case of 1VCe, which does not form $CeVO_4$ below 700 °C in air, but possesses a $CeVO_4$ phase after use in ethane ODH operation at temperatures not higher than 610 °C. This is also consistent with the effect of reducing environments that facilitate by ca. 200 °C the formation of $CeVO_4$ on ceria-supported vanadia [37]. The rather constant yield to ethylene with vanadia coverage evidences a decrease in the specific activity per vanadium site. This is in line with the increasing facility to react forming $CeVO_4$ as vanadia loading increases. For given reaction conditions, higher vanadia loading would afford a more extensive formation of $CeVO_4$. This would decrease the number of active sites available. A study is now on course to evaluate this issue.

5. Conclusions

VO_x/CeO_2 catalysts show highly dispersed surface vanadia species on CeO_2. The product distribution of VO_x/CeO_2 catalysts approaches that of $CeVO_4$ as vanadia loading increases. It appears that the same functionality (V^{5+}–O–Ce^{3+} bond) is present on both, ceria-supported vanadia and $CeVO_4$. The V^{5+}–O–Ce^{3+} site appears already from low temperature (300 °C) under air but temperature and vanadium loading facilitate the nucleation of a bulk-like $CeVO_4$ phase. The possibility of readily switching between Ce^{3+} and Ce^{4+} affords the vanadia–ceria solid-state reaction into $CeVO_4$. This is consistent with the remarkable ability of surface vanadia to remove the most easily reducible surface oxygen of CeO_2 and the inappreciable reduction of V^{5+} species at any ethane ODH reaction temperature.

Unlike most supported vanadia catalysts, the catalytic redox cycle in ceria-supported vanadia appears to be due to that of cerium sites near vanadium sites. Vanadium would moderate the lability of ceria oxygen sites. In addition, the redox cycle of Ce^{+3}/Ce^{4+} sites during ethane ODH reaction would be the driving force to enable the formation and growth of $Ce^{3+}V^{5+}O_4$ from $V^{5+}/Ce^{4+}O_2$ at temperatures lower than those observed in air.

Acknowledgments

This research was partially supported by the Ministry of Science and Technology Spain (Project MAT-2002-04000-CO2-01). J.M.C. thanks the *Ramón y Cajal* program for financial support. The SRS staff (Dr. I Harvey) at beamline 9.3 and EU support (Large Scale Facility Program, Project 39021) for performing XAFS measurements are fully appreciated.

References

[1] A. Trovarelli, Catal. Rev.-Sci. Eng. 38 (1996) 439.
[2] M.A. Bañares, X. Gao, J.L.G. Fierro, I.E. Wachs, Stud. Surf. Sci. Catal. 110 (1997) 295.
[3] W. Daniell, A. Ponchel, S. Kuba, F. Anderle, T. Weingand, D.H. Gregory, H. Knözinger, Top. Catal. 20 (2002) 65.
[4] M.A. Bañares, Catal. Today 51 (1999) 319.
[5] V.V. Guliants, Catal. Today 51 (1999) 255.
[6] I.E. Wachs, B.M. Weckhuysen, Appl. Catal. A 157 (1997) 67.
[7] E.A. Mamedov, V. Cortés Corberán, Appl. Catal. A 127 (1995) 1.
[8] T. Blasco, J.M.L. Nieto, Appl. Catal. A 157 (1997) 117.
[9] I.E. Wachs, J.M. Jehng, B.M. Weckhuysen, V.V. Guliants, J.B. Benziger, Catal. Today 32 (1996) 47.
[10] Q. Sun, J.M. Jehng, H.C. Hu, R.G. Herman, I.E. Wachs, K. Klier, J. Catal. 165 (1997) 91.
[11] M.A. Bañares, I.E. Wachs, J. Raman Spectroscopy 33 (2002) 359.
[12] M.A. Bañares, M.V. Martínez-Huerta, X. Gao, J.L.G. Fierro, I.E. Wachs, Catal. Today 2116 (2000) 1.
[13] M.A. Bañares, M.V. Martínez-Huerta, X. Gao, I.E. Wachs, J.L.G. Fierro, Stud. Surf. Sci. Catal. 130 (2000) 3125.
[14] T. Feng, J.M. Vohs, J. Catal. 221 (2004) 619.
[15] A.R. González-Elipe, F. Yubero, in: H.S. Nalwa (Ed.), Surface and Interface Analysis and Properties, in: Handbook of Surfaces and Interfaces of Materials, vol. 2, Academic Press, San Diego, 2001, p. 147.
[16] I.E. Wachs, Catal. Today 27 (1996) 437.
[17] U. Opara-Krasovec, B. Orel, A. Surca, N. Bukovec, R. Reisfelfd, Solid State Ionics 118 (1999) 195–214.
[18] M. Fernández-García, Catal. Rev. 44 (2002) 59.
[19] J. Wong, F. Lytle, R.P. Messmer, D.H. Maylotte, Phys. Rev. B 30 (1984) 5596.
[20] P. Concepción, H. Knözinger, J.M. López-Nieto, A. Martínez-Arias, J. Phys. Chem. B 106 (2002) 2574.
[21] R. Cousin, S. Capelle, E. Abi-Aad, D. Courcot, A. Aboukaïs, Chem. Mater. 13 (2001) 3862.
[22] R. Cousin, M. Dourdin, E. Abi-Aad, D. Courcot, S. Capelle, M. Guelton, A. Aboukaïs, J. Chem. Soc., Faraday Trans. 93 (1997) 3863.
[23] J. Matta, D. Courcot, E. Abi-Aad, A. Aboukaïs, Chem. Mater. 14 (2002) 4118.

[24] C. Oliva, G. Termignonne, F.P. Vatti, L. Forni, A.V. Vishniakov, J. Mater. Sci. 31 (1996) 6333.
[25] M. Figaj, K.D. Becker, Solid State Ionic 141–142 (2001) 507.
[26] A. Martínez-Arias, M. Fernández-García, L.N. Salamanca, R.X. Valenzuela, J.C. Conesa, J. Soria, J. Phys. Chem. B 104 (2000) 4035.
[27] A. Martínez-Arias, M. Fernández-García, O. Gálvez, J.M. Coronado, J.A. Anderson, J.C. Conesa, J. Soria, G. Munuera, J. Catal. 195 (2000) 207.
[28] M. Che, A.J. Tench, Adv. Catal. 31 (1982) 77.
[29] J.M. Coronado, A.J. Maira, A. Martínez-Arias, J.C. Conesa, J. Soria, J. Photochem. Photobiol. 150 (2002) 213.
[30] J. Soria, J.M. Coronado, J.C. Conesa, J. Chem. Soc., Faraday Trans. 92 (1996) 1619.
[31] N.I. Moiseeva, A.E. Gekhman, V.V. Minin, G.M. Larin, M.E. Bashtanov, A.A. Krasnovskii, I.I. Moiseev, Kinet. Catal. 41 (2000) 191.
[32] J. Xu, S.H. Overbury, J. Catal. 222 (2004) 167.
[33] J.P. Holgado, G. Munuera, J.P. Espinós, A.R. González-Elipe, Appl. Surf. Sci. 158 (2000) 164.
[34] G.S. Wong, J.M. Vohs, Surf. Sci. 498 (2002) 266.
[35] S. Tsunekawa, K. Ishikawa, Z.Q. Li, Y. Kawazoe, A. Kayusa, Phys. Rev. Lett. 85 (2000) 3440.
[36] M. Ji, M.S. Park, D.Y. Hong, J.S. Chang, S.E. Park, personal communication.
[37] M.V. Martínez-Huerta, PhD dissertation, Universidad Autónoma de Madrid, Spain (2001).